Metalurgi (2023) 3: 83 - 94

BRIN BADAN RISET DAN INOVASI NASIONAL

METALURGI
Majalah Ilmu dan Teknologi
p-ISSN 0126-3188 | e-ISSN 2443-3926
ejurnalmaterialmetalurgi.lipi.go.id

THE EFFECT OF AlTi5B1 AND ALTAB Ti80 WITH A COMBINATION OF AlSr15 AND Mg ADDITIONS ON STRENGTH AND DUCTILITY OF A356 ALUMINUM ALLOYS

Afghany Mostavan[a,*], Asep Ridwan[b], Arif Basuki[b], Husaini Ardy[b]

[a]Doctoral Program of Materials Science and Engineering
[a,b]Department of Materials Science and Engineering, Faculty of Mechanical and Aerospace Engineering
Institut Teknologi Bandung
Jl. Ganesha 10, Bandung, Indonesia 40132
*E-mail: 33720001@mahasiswa.itb.ac.id

Received: 20-05-2023, Revised: 16-11-2023, Accepted: 20-11-2023

Abstract

The current study aims to analyze microstructural changes affecting the A356 aluminum alloy, a hypoeutectic Al-Si-Mg alloy. This aluminum alloy is well-known for its strength, resistance to corrosion, lightweight, and heat treatability. The main objective of this research is to improve the strength and ductility of A356 alloys by using a synergistic strategy that includes AlTi5B1 and ALTAB Ti80 for microstructural alteration in combination with AlSr15 and Mg. The experimental results show that including all constituents in the as-cast condition enhances the ultimate tensile strength and elongation. Furthermore, in the heat-treated state, the addition of ALTAB Ti80 effectively maintains tensile strength (σ_{uts}=233.7 MPa), yield strength (σ_y=180.3 MPa), and elongation (e=5.8%). Additionally, when combined with Mg, the tensile strength and yield strength exhibit further improvement (σuts=253 MPa and σy=215.7 MPa); however, elongation is significantly reduced (e=2.7%).

Keywords: *A356 alloy, microstructure modification, mechanical properties*

1. INTRODUCTION

The A356 aluminum alloy, which is classified in the hypoeutectic group of the Al-Si phase diagram, is widely used in a variety of industrial sectors. Referred to as type AC4CH (JIS) and AlSi7Mg (ISO/DIN), A356 exhibits favorable characteristics during metal mold filling, possessing excellent mechanical properties, high resistance to dynamic loads, and exceptional corrosion resistance [1]. Hence, it is commonly used to fabricate pump housings, impellers, blowers, aircraft components, and vehicle parts [2]-[3].

The A356 aluminum alloy is widely used in the automobile sector, particularly in the production of cast wheel vehicles using GDC (gravity die casting) and LPDC (low-pressure die casting) techniques [4]. The quality of these casting wheel vehicles is influenced by factors such as alloy composition, casting process techniques, cooling rate, and heat treatment [5]. Specifications for casting wheels necessitate specific requirements, including a minimum ultimate tensile strength (σuts) of 277 MPa, minimum yield strength (σy) of 200 MPa, minimum elongation (e) of 7-12%, and a hardness range of 80-95 HB [4]-[6]. The ASTM B108 standard specifies the minimum ultimate tensile strength (σ_{uts}) of 260 MPa, the minimum yield strength (σ_y) of 150 MPa, and the minimum elongation (e) of 3% for aluminum alloy A356 after it completed the T6 heat treatment[8]. However, it is worth noting that A356 alloy exhibits high strength but low ductility, necessitating simultaneous enhancement of both properties.

The mechanical characteristics of aluminum alloys, particularly A356, are primarily determined by microstructure, morphology, grain

DOI : 10.55981/metalurgi.2023.714

Metalurgi is Sinta 2 Journal (https://sinta.kemdikbud.go.id/journals/profile/3708) accredited by Ministry of Education, Culture, Research, and Technology, Republic Indonesia

size, and phase distribution. Microstructural modifications are accomplished through various processing techniques such as casting, heat treatment, and the addition of alloying elements. Microstructural modifications in the A356 aluminum alloy can be produced by refining the grain structure with titanium (Ti) and boron (B), altering the morphology of the eutectic silicon (Si) precipitate phase using strontium (Sr) [7]-[10], and inducing precipitation hardening in magnesium (Mg) [11]-[12]. Refinement of the microstructure leads to a finer equiaxed structure, resulting in enhanced mechanical properties, improved castability, increased feed during solidification, reduced shrinkage porosity, and better dispersion of secondary phases [13]-[14]. The morphological properties of silicon (Si) particles in Al-Si-Mg alloys have a crucial role in improving their mechanical properties. The addition of strontium (Sr) significantly changes the microstructure of the eutectic silicon phase, transforming it from a coarse plate-like network to a finely dispersed fiber-like network [15].

In practical applications, grain refinement in casting aluminum alloys is commonly achieved through the use of grain refiners. The solidification process, which involves the nucleation and growth of alpha (α)-aluminum (Al), changes the grain size of an aluminum alloy. Effective grain refinement has been observed by adding Al-Ti-B refiners [16]-[18]. Existing literature demonstrates that grain refiners containing TiAl3, TiB2, and AlB2 particles exhibit superior grain refinement to those containing single particles[19]-[20]. Moreover, the T6 heat treatment of A356 aluminum alloy leads to a modification in the morphology of the eutectic silicon (Si) particles, changing from a plate-shaped configuration to a spherical form. This modification significantly impacts the alloy's mechanical properties, particularly its elasticity [21]-[23].

The design and development of ALTAB Ti80, an Al-Ti grain refiner, for refining cast aluminum alloys is novel in this work, presenting a potential alternate technique to grain refinement. Furthermore, the study investigates the combined effect of Sr and Mg in the A356 alloy, to improve its mechanical properties as well as provide novel possibilities for improving the material's strength and ductility. The study highlights the higher grain refinement achieved with specific particles (TiAl3, TiB2, and AlB2) as compared to single particles, revealing their critical role in the process. Further, the investigation clarifies the transformative effect of strontium (Sr) on the eutectic silicon (Si) phase's microstructure. To further improve our understanding of the phase properties of the alloy, it also examines how the T6 heat treatment affects the morphology of eutectic Si particles.

2. MATERIALS AND METHODS

2.1 Melt Preparation

The experimental procedure included melting an A356 aluminum alloy ingot in a 200 kg electric resistance furnace that was kept at a temperature of 720 ± 10 °C for 2-3 hours. To remove contaminants and avoid the formation of slag on the surface of the molten metal, Flux 4363 was added to the melt. Then, for five minutes, the molten metal was exposed to 3–5 kg/cm² of nitrogen gas as part of a degassing procedure. Subsequently, the molten metal was transferred to a small crucible with a capacity of 1.25 kg.

The desired compositions of the alloy samples, denoted as A1, A2, A3, and A4, were obtained by adding specific combinations of AlTi5B1, ALTAB Ti80, AlSr15, and magnesium to the molten metal in the small crucible. The composition of A1 was achieved by adding 1.5 gr of AlTi5B1 and 0.75 gr of AlSr15. A2 was obtained by incorporating 1.5 gr of AlTi5B1, 0.75 gr of AlSr15, and 1.5 gr of magnesium. Similarly, A3 was prepared by adding 1.25 gr of ALTAB Ti80 and 0.75 gr of AlSr15, while A4 was obtained by introducing 1.25 gr of ALTAB Ti80, 0.75 gr of AlSr15, and 1.5 gr of magnesium. The chemical compositions of the resultant alloys were analyzed using OES (optical emission spectrometry) Shimadzu and are outlined in Table 1.

Table 1. OES (weight percentage, wt.%) chemical composition of experimental alloys

ITEM	CHEMICAL INGREDIENT (wt.%)							
	Si	Mg	Fe	Mn	Cu	Zn	Ti	Sr
A0 (A356, base alloy)	7.05	0.43	0.09	0.002	0.002	0.02	0.14	0.010
A1 (A356+ AlTi5B18 + AlSr15)	7.00	0.43	0.08	0.002	0.002	0.02	0.14	0.013
A2 (A356+AlTi5B1 + AlSr15 + Mg)	6.96	0.48	0.08	0.002	0.002	0.02	0.15	0.011
A3 (A356+ALTAB Ti80 + AlSr15)	7.02	0.37	0.08	0.003	0.002	0.02	0.14	0.008
A4 (A356+ALTAB Ti80 + AlSr15 + Mg)	7.34	0.50	0.08	0.003	0.002	0.02	0.14	0.010

2.2 Casting Process and Heat Treatment

Tensile test specimens are produced by pouring molten aluminum at 720 °C into a permanent mold constructed following ASTM B-108 standards. Each casting yielded two tensile test bars, as depicted in Fig. 1(a). The alloys were melted and transferred into a crucible before being poured into the permanent mold using the gravity casting method, as illustrated in Fig. 1(b).

(a)

(b)

Figure 1. (a) Permanent tensile mold made following ASTM B-108, (b) manual gravity casting

Before casting, the mold was preheated to 300 °C. Five consecutive castings were conducted, each lasting 15 minutes, to produce specimens representing the A0, A1, A2, A3, and A4 conditions.

The cast tensile test bars were placed through T6 heat treatment, as shown in Fig. 2, which included solution treatment and artificial aging, with a period of ambient storage. After the specimens were heated to a temperature of 530 °C ± 20 °C for five to six hours to achieve the desired solution condition, they were immediately quenched in water before being returned to room temperature. Thereafter, the aging process was carried out for four to five hours at 160 °C ± 20 °C, and the air was cooled to room temperature.

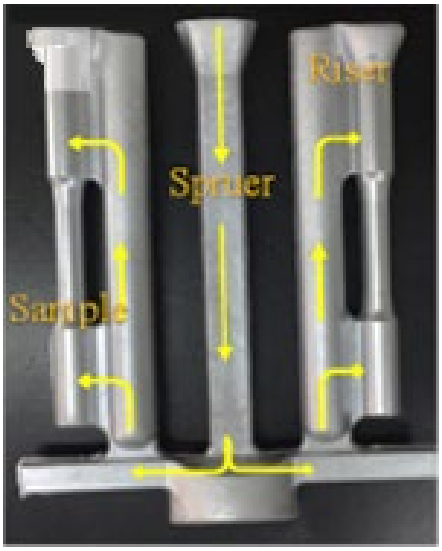

Figure 2. The round tensile test bar after heat treatment

Tensile tests were performed using a Gotech GT-7001-LCU Universal Computer Testing Machine following ASTM B557 standards. All of the examinations were carried out at room temperature. The gauge length of the extensometer was set to 45 mm, and the extension was applied at a ramp rate of 1 mm/min. Each reported data point is accompanied by a standard deviation derived from 3 to 5 samples' properties.

Optical microscopy observations were conducted on polished specimens without etching. The resulting metallographic images obtained from OM (optical microscope) were quantitatively measured using the Image J software application. For SEM (scanning electron microscope) analysis, the specimens were etched with 15 vol.% HCl before the examination.

3. RESULT AND DISCUSSION

3.1 Microstructure

Figure 3 shows the effect of AlTi5B1, ALTAB Ti80, AlSr15, and Mg additions on the microstructure of the as-cast and heat-treated A356 alloy. The dominant phase observed was α-Al, owing to the high solute content of the alloys, particularly with a silicon (Si) content of approximately 7 wt.%.

The OM (optical microscope) images in Fig. 3 depict the morphological variations of the as-cast A356 alloys, which were modified with AlTi5B1, ALTAB Ti80, AlSr15, and Mg, respectively. According to Fig. 3 - A0, the α-Al phase has a coarse dendritic morphology in the cast condition, but dendritic growth leads to an equiaxed structure in the heat-treated condition. The effect of AlTi5B1 on the primary α-Al phase (Figs. 3 A1 and A2) is comparable to that of the combination with ALTAB Ti80 (Figs. 3 A3 and A4). The addition of AlTi5B1 and ALTAB induces the rapid dissolution of Al3Ti particles within the melt, facilitating the incorporation of Ti solute elements to hinder subsequent grain growth. Concurrently, TiB2 particles provided by AlT5B1 serve as effective heterogeneous nucleation centers, offering suitable substrates for refining the grain structure [24]-[25].

Furthermore, the alloys exhibit fine acicular silicon (Si) precipitates in the as-cast condition, indicating successful modification of the eutectic Si phase. As a result of the solution treatment during homogenization, the eutectic Si phase transitions from fine acicular to spheroidal precipitates in the heat-treated condition. After heat treatment, the Sr-modified alloy exhibits clear microstructural changes, such as a decrease in block primary Si and a rounding of the needle-like eutectic Si. Furthermore, the addition of Sr causes the grains to form more uniformly and equiaxed [15], [26].

The properties of the α-Al phases and the Si eutectic phase were evaluated quantitatively. Figures 4 and 5 show the results of these measurements, which show the microstructural state in the as-cast condition before any T6 heat treatment. Figures 6 and 7 also provide information on the microstructural development after the T6 heat treatment. After the T6 treatment, the α-Al phases grew significantly, which coincided with a clear morphological change of the Si precipitates into a spheroidal shape.

A further comprehensive analysis was conducted employing optical micrographs, as presented in Figures 4, 5, 6, and 7. These exhibits effectively summarize the investigation focused on the primary α-Al phase and Si eutectic precipitates within the A356 alloys, which are distinguished by different compositions involving AlTi5B1, ALTAB Ti80, AlSr15, and Mg. The as-cast A356 alloy's initial α-Al phase had a coarse dendritic morphology. The Image J application was used to quantify the dimensions of both the α-Al phase and the Si eutectic phase, providing for a robust statistical distribution analysis.

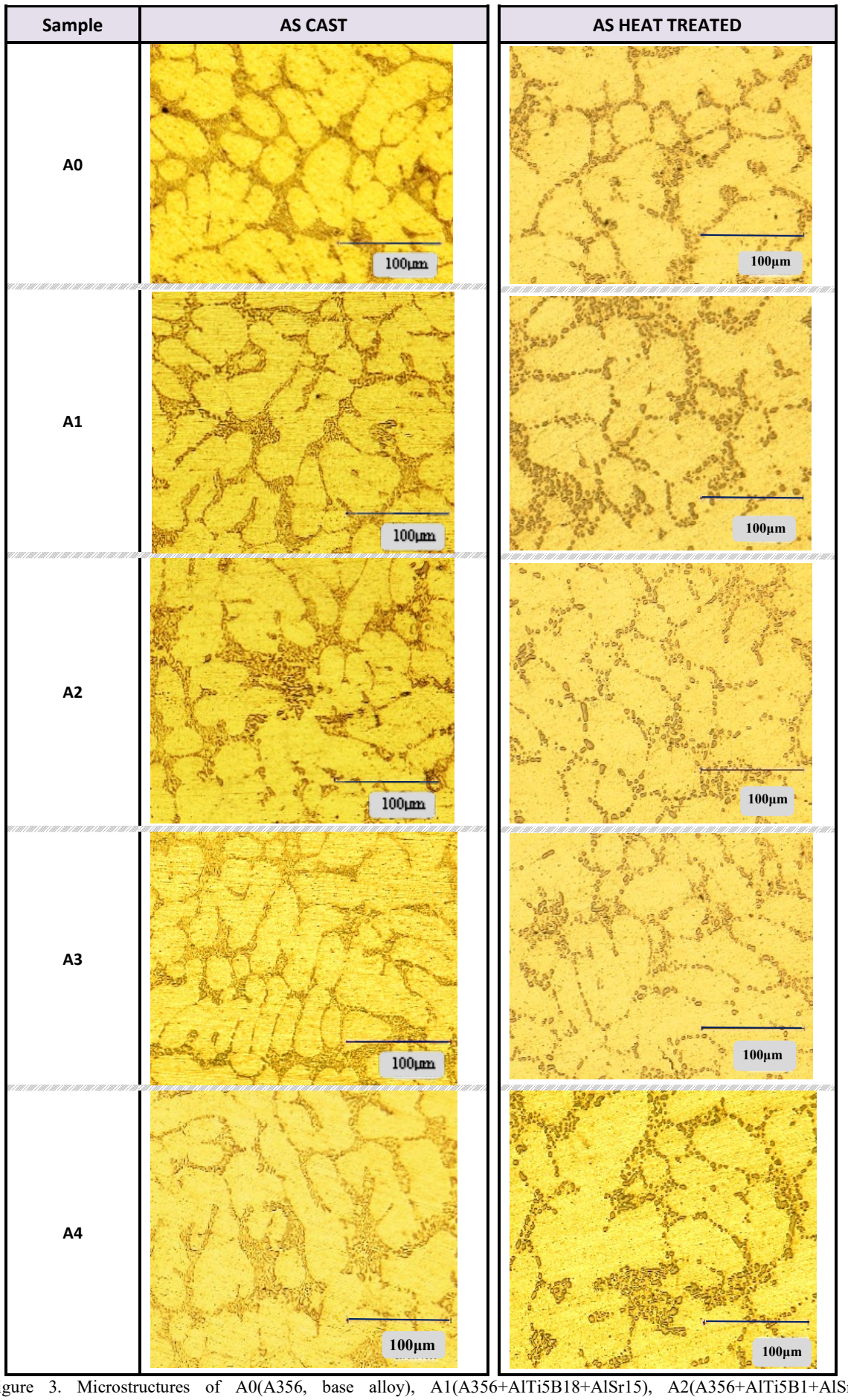

Figure 3. Microstructures of A0(A356, base alloy), A1(A356+AlTi5B18+AlSr15), A2(A356+AlTi5B1+AlSr15+Mg), A3(A356+ALTAB Ti80+AlSr15), A4(A356+ALTAB Ti80+AlSr15+Mg) before (as cast) and after T6 (as heat treated) with 1000x magnification

Figure 4 shows the examination of the size area distribution of the primary α-Al phase in the casting condition. Without any combination, the distribution is centered around 1500 µm. However, when combined with AlTi5B1 or ALTAB Ti80, the distribution spreads to a range of 2000 to 3000 µm. A slight difference is observed when comparing the size area distribution of the primary α-Al phase with and without the addition of AlTi5B1 or ALTAB Ti80, indicating that these additions do not cause a significant change in the α-Al phase, as expected for grain refinement in the A356 alloy.

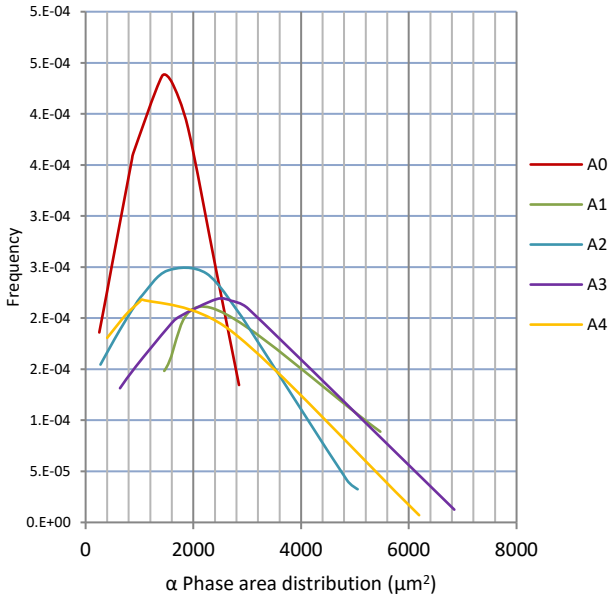

Figure 4. The curve in the α phase size area distribution A0(A356, base alloy), A1 (A356+AlTi5B18+AlSr15), A2(A356+AlTi5B1+AlSr15+Mg), A3(A356+ALTAB Ti80+AlSr15), A4 (A356+ALTAB Ti80+AlSr15+Mg) as cast

Previous research [19], [21] has shown that adding Ti atoms to the A356 alloy causes the formation of Al3Ti precipitates as Ti reacts with Al atoms in the melt. An increase in Ti concentration corresponds to the formation of larger Al3Ti particles. As a result, the dimensions of the primary α–Al phase should be reduced. Nonetheless, within the scope of this investigation, the observed size distribution of the primary α–Al phase indicates that the addition of AlTi5B1 or ALTAB Ti80 has no significant effect on the grain size of the α–Al phase.

The size area distribution of the primary Si eutectic phase in the casting state, which ranges from 15 to 20 µm², is shown in Fig. 5. Among the important findings is the result that the Si eutectic phase's size area distribution does not significantly change under any of the various sample conditions examined.

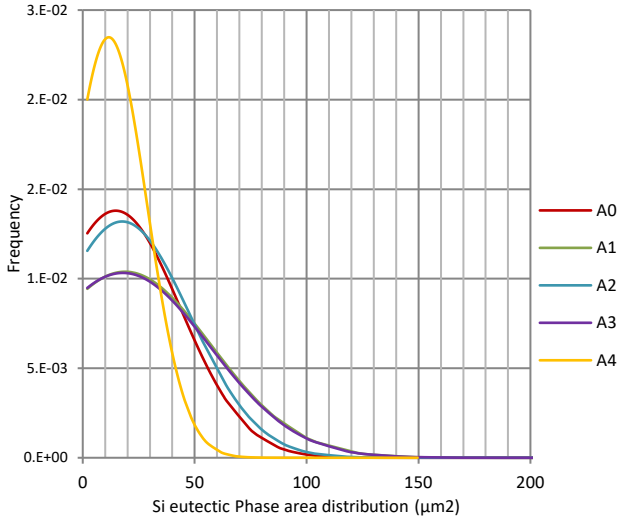

Figure 5. The curve in the Si eutectic phase size area distribution A0(A356, base alloy), A1(A356+AlTi5B18+AlSr15), A2 (A356+AlTi5B1+AlSr15+Mg), A3 (A356+ALTAB Ti80+AlSr15), A4 (A356+ALTAB Ti80+AlSr15+Mg) as cast

Figures 6 and 7 show the analysis of size area distribution after T6 heat treatment, which is an important factor for determining the mechanical strength of cast aluminum alloys. The strength characteristics of these alloys are effectively influenced by parameters such as grain size, secondary phase grain, and precipitation hardening.

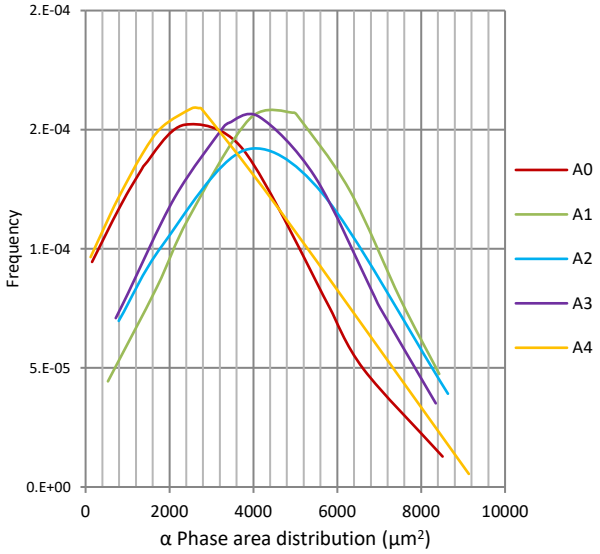

Figure 6. The curve in the α phase size area distribution A0(A356, base alloy), A1(A356+AlTi5B18+AlSr15), A2(A356+AlTi5B1+AlSr15+Mg), A3(A356+ALTAB Ti80+AlSr15), A4 (A356+ALTAB Ti80+AlSr15+Mg) as heat treated

Figure 6 shows a growth in the size area distribution of the α–Al phase post-T6 heat treatment relative to the as-cast state, indicating an enlargement in the dimensions of the α–Al phase due to thermal processing. As compared to the as-cast state, Fig. 7 illustrates a decrease in the Si eutectic phase's size area distribution after T6 heat treatment. This suggests that the thermal treatment processes have reduced the size of the Si eutectic phase.

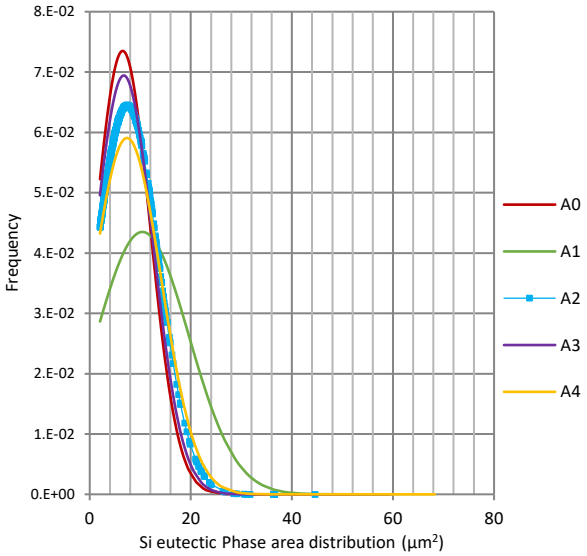

Figure 7. The curve in the Si eutectic phase size area distribution A0(A356, base alloy), A1(A356+AlTi5B18+ AlSr15), A2 (A356+AlTi5B1+AlSr15+Mg), A3 (A356+ ALTAB Ti80+AlSr15), A4 (A356+ALTAB Ti80+AlSr15+ Mg) as heat treated

3.2 Mechanical Properties

The effects of adding AlTi5B1, ALTAB Ti80, AlSr15, and Mg on the A356 alloy's ultimate tensile strength (UTS) and elongation (%) are shown in Figures 8 and 9. The results indicate that the introduction of these combinations does not yield enhancements in the strength properties compared to the as-cast condition (A0). However, an increase in elongation is observed when ALTAB Ti80 is added to the alloy.

The results of the tensile testing, presented in Fig. 8, provide insights into the tensile strength and elongation values for each combination variation. The graph shows that the tensile strength and elongation strength values have a slight similarity. An addition of ALTAB Ti80 remarkably results in an elevated elongation value of 6.5%. In this case, the ultimate tensile strength is 167 MPa, and the yield strength is 96 MPa. The addition of AlTi5B1 results in an elongation of 5.6%, an ultimate tensile strength of 166 MPa, and a yield strength of 83 MPa.

However, the addition of magnesium (Mg) to these aluminum alloys reduces elongation for specimens subjected to the AlTi5B1 condition, with no significant change observed in specimens subjected to the ALTAB Ti80 condition.

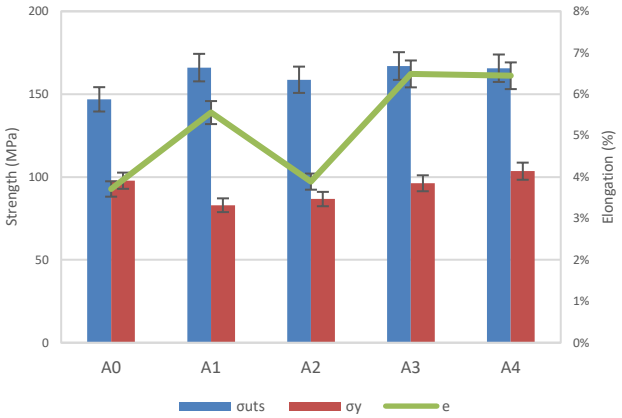

Figure 8. Results of tensile strength and elongation A0(A356,base alloy), A1(A356+AlTi5B18+AlSr15), A2(A356+AlTi5B1+ AlSr15+Mg), A3(A356+ALTAB Ti80 +AlSr15), A4(A356+ALTAB Ti80+AlSr15+Mg as cast

Figure 9 shows that the application of T6 heat treatment affects the tensile strength and elongation of the A356 alloy. Heat treatment increases tensile strength while decreasing elongation, which is primarily due to the formation of intermetallic phases. Indeed, among the tested variations, the unalloyed A356 alloy has the lowest tensile strength. In the heat-treated condition, the ALTAB Ti80 variation displays the highest elongation value of 5.8%, followed by AlTi5B1 with an elongation of 3.4%. The addition of Mg to the alloy reduces elongation, with the Mg-containing variant having an elongation value of 2.7%.

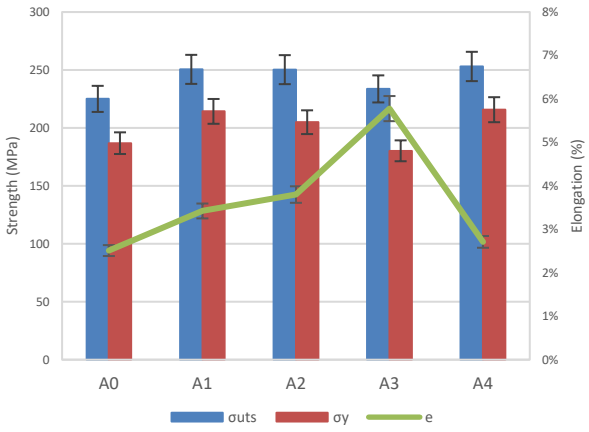

Figure 9. Results of tensile strength and elongation A0 (A356,base alloy), A1(A356+AlTi5B18+AlSr15), A2 (A356+AlTi5B1+AlSr15+Mg), A3(A356+ALTAB Ti80+ AlSr15), A4(A356+ALTAB Ti80+AlSr15+Mg) as heat treated

Figure 10 shows the difference in microhardness between the α-Al phase and the Si eutectic phase. The micro Vickers hardness test results indicate that, in the as-cast condition, the eutectic phase has higher hardness than the α-Al phase.

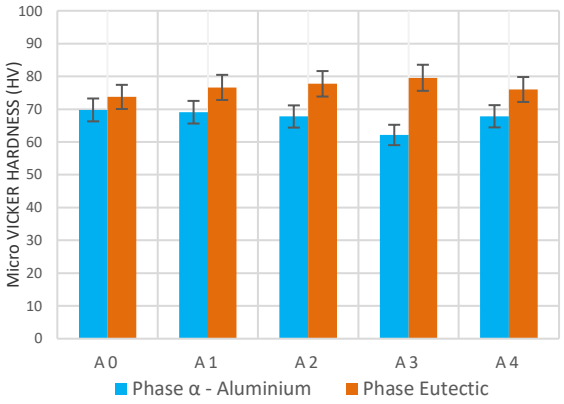

Figure 10. Results of micro Vickers hardness A0(A356, base alloy), A1(A356+ AlTi5B18 + AlSr15), A2(A356+AlTi5B1 +AlSr15+Mg), A3(A356+ALTAB Ti80+AlSr15), A4(A356 +ALTAB Ti80+AlSr15+Mg) as cast

Following the heat treatment T6 process in Fig.11, a notable enhancement in hardness was observed in both phases, with the α-Al phase exhibiting greater hardness than the eutectic phase. This outcome aligns with previous research indicating that the T6 heat treatment can promote grain growth. Additionally, the inclusion of Mg led to the formation of the Mg_2Si intermetallic compound, which contributed to the increased hardness.

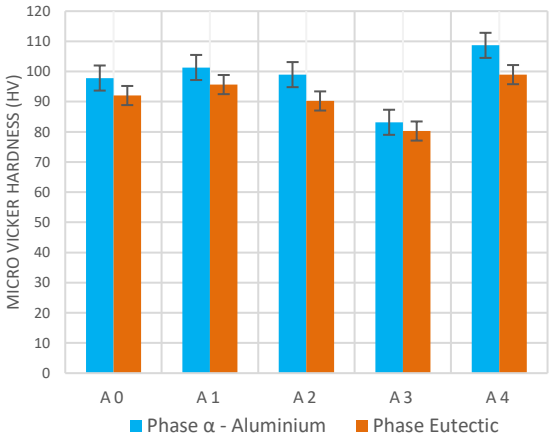

Figure 11.Results of micro Vickers hardness A0 (A356,base alloy), A1(A356+AlTi5B18+AlSr15), A2(A356+AlTi5B1+AlSr15+Mg), A3(A356+ALTAB Ti80+AlSr15), A4(A356+ALTAB Ti80+AlSr15+Mg) as heat treated

n
e
e

A356 aluminum alloys containing additions of ALTAB Ti80 and AlSr15, as illustrated in Fig. 12. The ensuing analysis unveiled that throughout the heat treatment sequence, silicon (Si) and strontium (Sr) elements were predominantly localized within the boundary zones encompassing the α-Al matrix. Conversely, magnesium (Mg), titanium (Ti), and iron (Fe) elements were found to be distributed within the α-Al matrix.

The revealed elemental distribution patterns hold notable implications for the alloy's fracture behavior. The concentration of Si and Sr at the α-Al matrix boundaries could potentially influence interfacial interactions and mechanical bonding, potentially affecting the alloy's fracture toughness. On the other hand, the dispersion of Mg, Ti, and Fe within the α-Al matrix suggests their potential involvement in the formation of strengthening phases or precipitates, which could contribute to altered fracture mechanisms.

The findings correspond with prior research [27]-[29]. The nucleation of silicon particles on the phase means that they formed early during solidification at high temperatures, acting as nucleation sites for Si particles. The simultaneous coexistence of acicular-shaped precipitates and silicon particles in the eutectic might occur from iron rejection into the remaining liquid during the solidification.

Illustrated in Fig. 13 are the fracture surfaces of A356 aluminum alloys subjected to modifications involving ALTAB Ti80 and AlSr15. Optical metallography and SEM (scanning electron microscope) techniques were used to characterize the fragments. Fracture initiation occurred within the inter-dendritic eutectic region, according to fracture feature analysis. The principal crack propagated through the biphasic domain, extending along the edge line. Within the α-Al solid solution phase, the presence of silicon (Si) precipitates induced the appearance of sharp edges and secondary cracks, indicative of a brittle behavior.

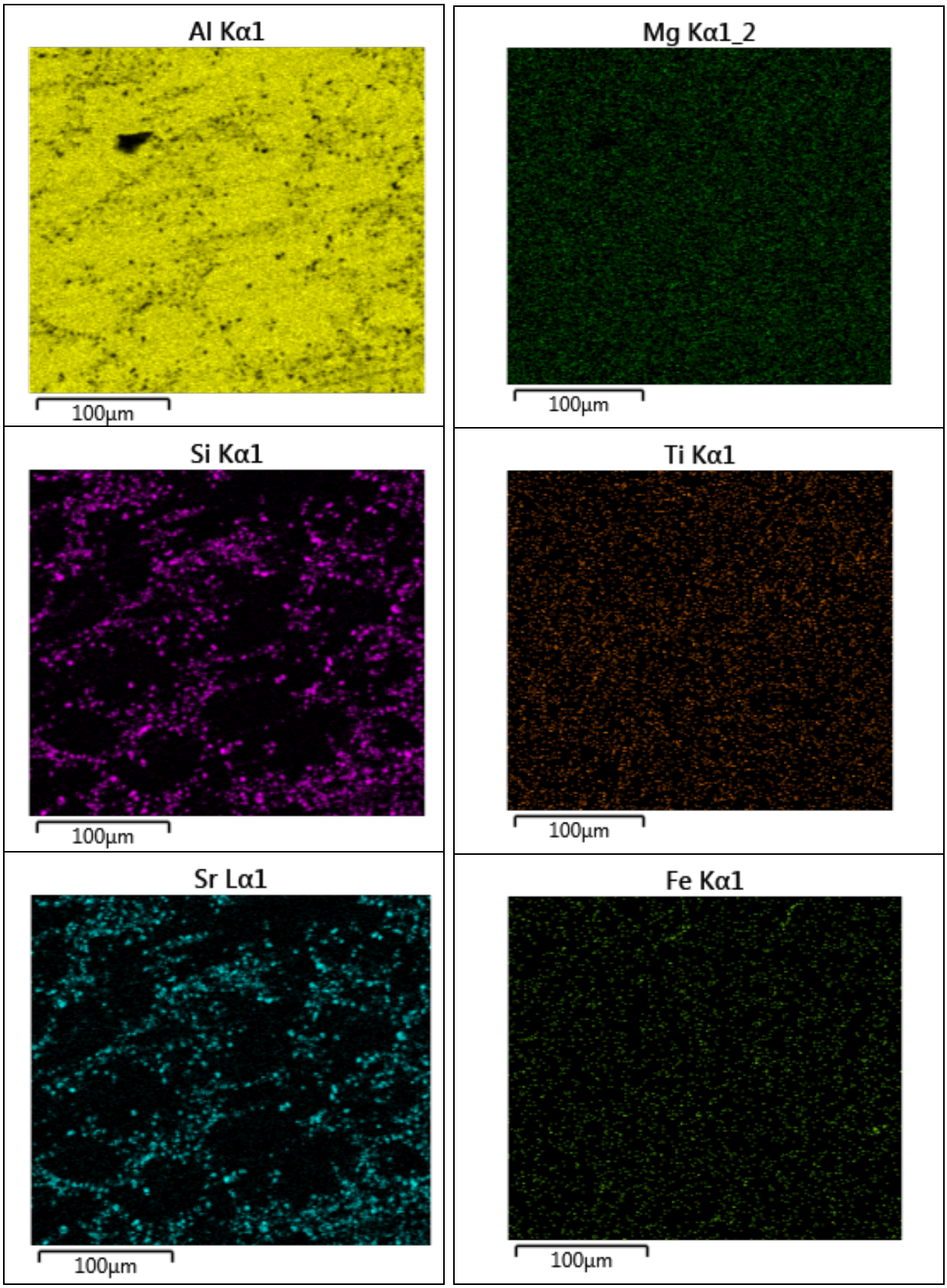

Figure 12. EDS mapping a typical region of A356 aluminum alloy (ALTAB Ti80 + AlSr15), T6 heat-treated state

The SEM analysis of the heat-treated A356 aluminum alloy (Fig. 14. (a)) revealed a distinctive cellular trans-crystalline fracture mechanism.

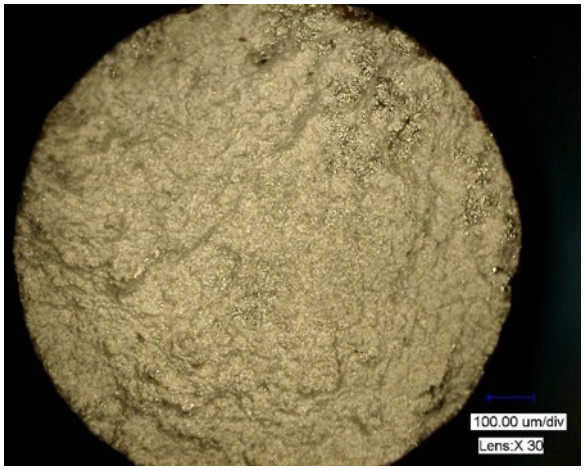

Figure 13. Fractography of the tensile A356 aluminum alloy (ALTAB Ti80 + AlSr15), T6 heat-treated state

This mode of fracture was typified by the development of micro-necks within the α-Al structure and a characteristic dimple structure morphology (Fig. 14(b)). Remarkably, this fracture pattern was consistently discerned across all samples encompassing distinct additive combinations.

The observed fracture characteristics offer insights into the alloy's mechanical behavior. The inter-dendritic eutectic region's tendency for fracture initiation suggests its susceptibility to stress concentration, potentially influencing the alloy's overall fracture toughness. The appearance of brittle features within the solid solution phase, attributed to Si precipitates, further emphasizes the alloy's weakness to rapid fracture under certain loading conditions. Conversely, the identified cellular trans-crystalline fracture pattern, consistently prevalent across diverse compositions, might be indicative of the alloy's inherent fracture mode, potentially linked to its microstructural attributes and mechanical properties.

As stated in another investigation [24], [30]-[31], the brittle fracture of the alloys is mainly caused by the fracture of the needle-like eutectic Si, with crack development starting at the silicon particles. In addition, examination of the fracture morphology and the existing cracks points to the possibility of intergranular fracture, where fissures propagate along the grain boundary during their fracture. The continuity of the grain boundary in the aluminum matrix is broken by the presence of substantial primary and eutectic Si. At this location, fracture development results from insufficient coordination of deformation between neighboring grains. The unaltered alloy's fracture surface has several smooth, flat areas that are divided by ripping ridges. The area of a smooth, flat surface decreases once the eutectic Si is modified, and this leads to grain refinement.

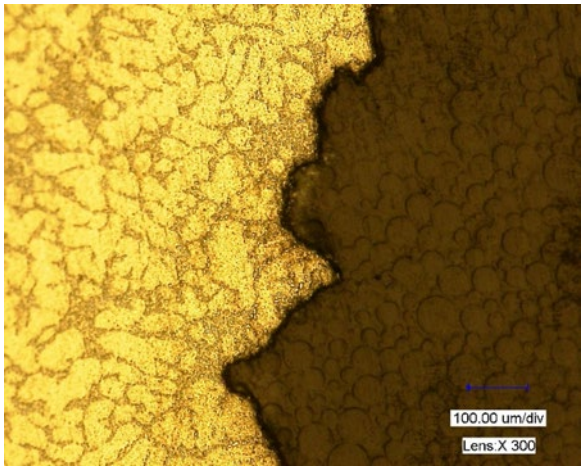

(a)

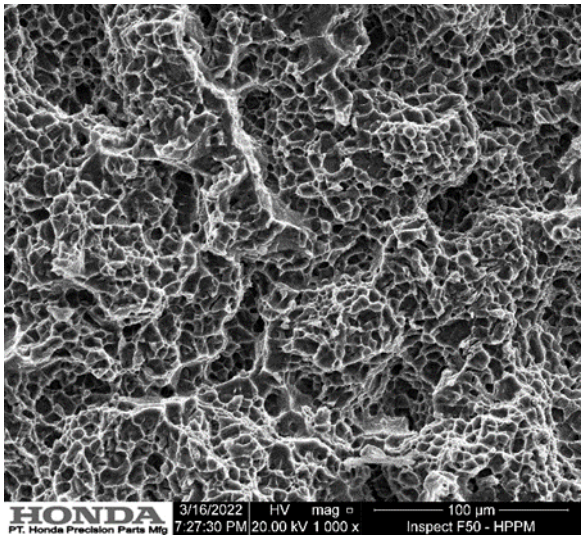

(b)

Figure 14. Observation of SEM for fractography of the tensile A356 aluminum alloy (ALTAB Ti80 + AlSr15), T6 heat-treated state; (a) Cross section, (b) Top surface

4. CONCLUSION

The addition of AlTi5B1, ALTAB Ti80, AlSr15, and 99% Mg ingot to the A356 aluminum alloy resulted in minor chemical modifications. Tensile test findings revealed that these combined components had a significant impact on the alloy's ductility (ε). T6 heat treatment enhanced tensile strength (σ_{UTS}) and yield strength (σ_y) but decreased ductility (ε), with ALTAB Ti80 having the best ductility value. Under as-cast circumstances, Sr modification enhanced the development of fine fibrous Si precipitates, which transitioned to spheroidized Si precipitates after the T6 heat treatment, according to microstructural examination. Micro Vickers hardness testing revealed that the eutectic phase had higher hardness than the α-aluminum phase,

with both phases having enhanced hardness after the T6 heat treatment, particularly the α-aluminum phase. In the A356 aluminum alloy, a fracture study after heat treatment revealed cellular trans-crystalline fractures with micro-necks and a dimple structure shape.

ACKNOWLEDGMENT

This research is part of a doctoral study conducted at the Institute of Technology Bandung (ITB) and has been financially supported by the Mayasari Bakti Utama Foundation. The authors gratefully acknowledge PT. Chemco Harapan Nusantara for providing the necessary samples experimental facilities and PT. Honda Precision Parts Manufacturing for access to SEM/EDS facilities, which greatly contributed to the success of this experiment.

REFERENCES

[1] X. Yang, C. Xu, R. Zheng, S. Guan, and C. Ma, "Towards strength-ductility synergy through an optimized thermomechanical treatment in hypoeutectic Al-Si alloys," *Mater. Lett.*, vol. 295, p. 129850, 2021. Doi: 10.1016/j.matlet.2021.129850.

[2] I. Polmear, D. StJohn, J.-F. Nie, and M. Qian, *Casting of Light Alloys*. 2017. Doi: 10.1016/b978-0-08-099431-4.00003-8.

[3] A. Graf, "Aluminum alloys for lightweight automotive structures," *Mater. Des. Manuf. Light. Veh.*, pp. 97–123, Jan. 2020. Doi: 10.1016/B978-0-12-818712-8.00003-3.

[4] J. Ou, C. Wei, S. Cockcroft, D. Maijer, L. Zhu, Lateng A, C. Li, and Z. Zhu, "Advanced process simulation of low-pressure die-cast a356 aluminum automotive wheels-part I, process characterization," *Metals (Basel)*, vol. 10, no. 5, 2020. Doi: 10.3390/met10050563.

[5] M. Kaba, A. Donmez, A. Cukur, A. F. Kurban, H. E. Cubuklusu, and Y. Birol, "AlSi5Mg0.3 alloy for the manufacture of automotive wheels," *Int. J. Met.*, vol. 12, no. 3, pp. 614-624, 2018. Doi: 10.1007/s40962-017-0191-2.

[6] European Aluminium Association, "Applications - chassis & suspension - wheels," *The Aluminium Automotive Manual*, 2011. https://european-aluminium.eu/wpcontent/uploads/2022/11/aam-applications-chassis-suspension-3-wheels.pdf, [Accessed, 1 December 2022)

[7] J. Ou, C. Wei, S. Cockcroft, D. Maijer, L. Zhu, Lateng A, C. Li, and Z. Zhu, "Advanced process simulation of low pressure die-cast a356 aluminum automotive wheels-part ii modeling methodology and validation," *Metals (Basel).*, vol. 10, no. 11, pp. 1-24, 2020. Doi: 10.3390/met10111418.

[8] ASTM Standard B 108/B108M - 08, *"Standard Specification for Aluminum-Alloy Permanent Mold Castings."* ASTM International, 2009.

[9] A. K. Dahle, K. Nogita, S. D. McDonald, C. Dinnis, and L. Lu, "Eutectic modification and microstructure development in Al-Si Alloys," *Mater. Sci. Eng. A*, vol. 413-414, pp. 243-248, 2005. Doi: 10.1016/j.msea.2005.09.055.

[10] H. Tahiri, S. S. Mohamed, H. W. Doty, S. Valtierra, and F. H. Samuel, "Effect of Sr–grain refining–Si interactions on the microstructural characteristics of Al-Si hypoeutectic alloys," *Int. J. Met.*, vol. 12, no. 2, pp. 343-361, 2018. Doi: 10.1007/s40962-017-0169-0.

[11] M. R. S. Ganesh, N. Reghunath, M. J.Levin, A. Prasad, S. Doondi, and K. V. Shankar, "Strontium in Al-Si-Mg Alloy: A review," *Metals and Materials Internationals*, vol. 28, pp. 1-40, 2022. Doi: 10.1007/s12540-021-01054-y.

[12] R. G. Guan and D. Tie, "A review on grain refinement of aluminum alloys: Progress, challenges, and prospects," *Acta Metall. Sin. (English Lett.)*, vol. 30, no. 5, pp. 409-432, 2017. Doi: 10.1007/s40195-017-0565-8.

[13] R. Chen, Q. Xu, H. Guo, Z. Xia, Q. Wu, and B. Liu, "Correlation of solidification microstructure refining scale, Mg composition and heat treatment conditions with mechanical properties in Al-7Si-Mg cast aluminum alloys," *Mater. Sci. Eng. A*, vol. 685, pp. 391-402, 2017. Doi: 10.1016/j.msea.2016.12.051.

[14] J. Santos, A. K. Dahle, and A. E. W. Jarfors, "Magnesium solubility in primary α-al and heat treatment response of cast Al-7Si-Mg," *Metals (Basel).*, vol. 10, no. 5, 2020. Doi: 10.3390/met10050614.

[15] E. Fracchia, F. S. Gobber, and M. Rosso, "Effect of alloying elements on the Sr modification of Al-Si cast alloys," *Metals*, vol. 11, no. 2, pp. 342, 2021. Doi: 10.3390/met11020342.

[16] B. T. Sofyan, D. J. Kharistal, L. Trijati, K. Purba, and R. E. Susanto, "Grain refinement of AA333 aluminum cast alloy by Al-Ti granulated flux," *Mater. Des.*, vol. 31, pp. S36-S43, 2010. Doi: 10.1016/j.matdes.2010.02.007.

[17] S. Derin, Y. Birol, and U. Aybarc, "Effect of strontium addition on microstructure and mechanical properties of AlSi7Mg0.3

alloy," *Int. J. Met.*, vol. 11, no. 4, pp. 688-695, 2017. Doi: 10.1007/s40962-016-0117-4.

[18] S. Suhariyanto, S. Hadi, M. Mursid, and G. D. W, "Mechanical property improvement for Aluminum alloy Al-7Si with additive material of Al-TiB and heat treatment of T5," *IPTEK J. Proc. Ser.*, no. 3, pp. 25, 2019. Doi: 10.12962/j23546026.y2019i3.5857.

[19] Y. Cui, D. J. M. King, A. P. Horsfield, and C. M. Gourlay, "Solidification orientation relationships between Al3Ti and TiB2," *Acta Mater.*, vol. 186, pp. 149-161, 2020. Doi: 10.1016/j.actamat.2019.12.013.

[20] A. M. Samuel, S. S. Mohamed, H. W. Doty, S. Valtierra, and F. H. Samuel, "Some aspects of grain refining of Al-Si cast alloys," *Int. J. Cast Met. Res.*, vol. 32, no. 1, pp. 1-14, 2019. Doi: 10.1080/13640461.2018.1498623.

[21] M. Emamy, M. Malekan, A. H. Pourmonshi, and K. Tavighi, "The influence of heat treatment on the structure and tensile properties of thin-section A356 aluminum alloy casts refined by Ti, B, and Zr," *J. Mater. Res.*, vol. 32, no. 18, pp. 3540-3547, 2017. Doi: 10.1557/jmr.2017.193.

[22] Q. Li, B. Li, J. Li, T. Xia, Y. Lan, and T. Guo, "Effects of the addition of Mg on the microstructure and mechanical properties of hypoeutectic Al-7%Si alloy," *Int. J. Met.*, vol. 11, no. 4, pp. 823-830, 2017. Doi: 10.1007/s40962-016-0131-6.

[23] E. Fracchia, F. S. Gobber, and M. Rosso, "Effects of casting-additives on the microstructure evolution of hypoeutectic aluminium-silicon alloys," *Metals (Basel).*, vol. 10, no. 5, 2020. Doi: 10.3390/met10050618.

[24] P. Tan, Y. Yang, Y. Sui, Q. Wang, and Y. Jiang, "The influence of Al-10Sr or/ and Al-5Ti-1B on microstructure and mechanical properties of Al-12Si-4Cu-2Ni-0.8 Mg alloys," *J. Alloys Compd.*, vol. 809, pp. 1-7, 2019. Doi: 10.1016/j.jallcom.2019.151856.

[25] D. G. Mallapur, S. A. Kori, and K. R. Udupa, "Influence of Ti, B, and Sr on the microstructure and mechanical properties of A356 alloy," *J. Mater. Sci.*, vol. 46, no. 6, pp. 1622-1627, 2011. Doi: 10.1007/s10853-010-4977-3.

[26] S. Haro-Rodríguez, R. E. Goytia-Reyes, D. K. Dwivedi, V. H. Baltazar-Hernández, H. Flores-Zúñiga, and M. J. Pérez-López, "On the influence of Ti and Sr on microstructure, mechanical properties and quality index of cast eutectic Al-Si-Mg alloy," *Mater. Des.*, vol. 32, no. 4, pp. 1865-1871, 2011. Doi: 10.1016/j.matdes.2010.12.012.

[27] R. Ghomashchi, "The evolution of AlTiSi intermetallic phases in Ti-added A356 Al-Si alloy," *J. Alloys Compd.*, vol. 537, pp. 255-260, 2012. Doi: 10.1016/j.jallcom.2012.04.087.

[28] Y. Hu, L. Zhao, D. Liu, Y. Tang, and H. Jiang, "Microstructural evolution of semi-solid A356 alloy during reheating," *Int. J. Mater. Res.*, vol. 109, no. 10, pp. 951-956, 2018. Doi: 10.3139/146.111691.

[29] D. Yong Wu *et al.*, "Utilizing a novel modifier to realize multi-refinement and optimized heat treatment of A356 alloy," *J. Alloys Compd.*, vol. 791, pp. 628-640, 2019. Doi: 10.1016/j.jallcom.2019.03.327.

[30] X. Dong, Y. Zhang, and S. Ji, "Enhancement of mechanical properties in high silicon gravity cast AlSi9Mg alloy refined by Al3Ti3B master alloy," *Mater. Sci. Eng. A*, vol. 700, pp. 291-300, 2017. Doi: 10.1016/j.msea.2017.06.005.

[31] X. Dong, Y. Zhang, S. Amirkhanlou, and S. Ji, "High-performance gravity cast Al9Si0.45Mg0.4Cu alloy inoculated with AlB2 and TiB2," *J. Mater. Process. Technol.*, vol. 252, pp. 604-611, 2018. Doi 10.1016/j.jmatprotec.2017.10.028